Journal of Physics: Conference Series **166** (2009) 012009 doi:10.1088/1742-6596/166/1/012009

Stability of a finite-length rivulet under partial wetting conditions

Javier A. Diez, Alejandro G. González

Instituto de Física Arroyo Seco,
Universidad Nacional del Centro de la Provincia de Buenos Aires - CONICET, Pinto 399, 7000, Tandil, Argentina

Lou Kondic

Department of Mathematical Sciences
Center for Applied Mathematics and Statistics
New Jersey Institute of Technology, Newark, NJ 07102

Abstract. We study the stability of a finite-length fluid rivulet at rest on a partially wetting surface. We consider the problem by including the intermolecular force (van der Waals interaction) within the framework of the lubrication approximation. The results are validated by comparison with numerical simulations of the full nonlinear equation. For finite length rivulets, we show that the distance between drops after breakup is very close to the wavelength of maximum growth rate predicted by the linear theory for infinite rivulets. Finally, we compare theoretical and numerical results with reported experimental data.

1. Introduction

The evolution of partially wetting thin liquid films on solid substrates and the subsequent pattern formation is a subject of growing importance. The interest on the subject is raised by a variety of important applications such as thin films in micro- and nano-fluidics [1, 2], as well as templating or lithographic patterning and various types of coatings [3, 4, 5]. Many of the fundamental dewetting studies have focused on continuous liquid or polymeric [6, 7] thin films. More recently, the dewetting characteristics of continuous thin metal films were studied [8]. In all of these examples, the films are often unstable and break up, leading to the formation of dry spots. One important question is what are the mechanisms involved in the dewetting and breakup of unstable thin films. The instability has been found to be either driven by nucleation at defect sites which are not spatially correlated, or via spinodal-type of instabilities resulting in a spatial correlation [9, 8, 10].

In this work we consider the instability of finite-length fluid rivulets placed on a horizontal substrate under partial wetting conditions (see Fig. 1). The case of an infinite rivulet has previously been considered by other authors assuming sharp contact lines and circular cross section shapes. Among the most relevant papers on the subject we mention the works by Davis [11], Langbein [12], Roy & Schwartz [13], Sekimoto et al. [14] and Brochard-Wyart et al. [7]. Here, we perform a stability analysis by considering van der Waals forces which diffuse the contact line into a thin precursor film and also consider the effects of gravity. Thus, the cross

section of the rivulet cannot be described as a circle either because of the non sharp contact line or because of the influence of gravity.

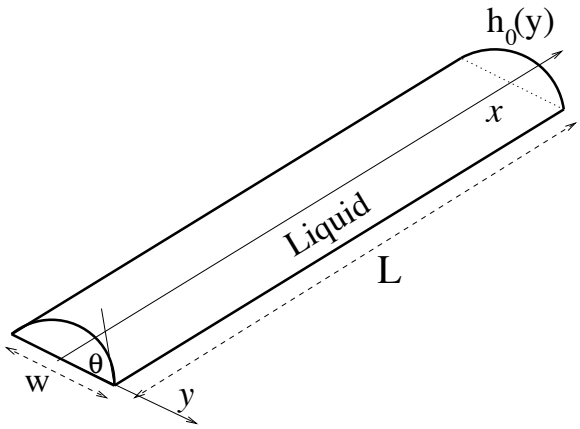

Figure 1. Schematic of the liquid rivulet placed on a horizontal substrate.

One significant difference to previous approaches is that intermolecular forces are taken into account. Here, we choose a conjoining/disjoining pressure model. Instead of imposing a fixed contact angle at the contact line where $h \to 0$, we introduce the wettability properties directly in the model so to reach a given free surface slope (apparent contact angle, θ) far from the contact line. To do so, an equilibrium film is required ahead of the macroscopic contact line, whose thickness is very close to that of equilibrium for an infinite flat film.

The paper is organized as follows. The linear stability analysis (LSA) within the framework of lubrication approximation is presented in Section 2. The comparison between the linear theory and the numerical evolution of the full nonlinear equation is given in Section 3, where the case of finite rivulet is also considered. The comparison between experimental data reported elsewhere and the present theoretical and numerical results is discussed in Section 4. Finally, Section 5 summarizes main results and conclusions.

2. Long-wave approximation and linear stability analysis

In the study of thin film flows on solid substrates, the evolution of the fluid thickness, h, is typically described under the framework of lubrication theory. This approach allows to reduce Navier-Stokes equations to a single nonlinear partial differential equation for h. In addition, finite contact angles can be included in the model by accounting for van der Waals forces, as described below.

We note that although lubrication theory is strictly valid only in the problems characterized by vanishing free surface slopes, it has been used commonly in partial wetting conditions, therefore in situations where the contact angle is not necessarily small [15, 16, 17]; see also [18, 19, 20, 21] for further discussion regarding involved issues. This approach has been justified in part by the works which show that even in the case of large contact angles, only relatively small deviations from more complete models result. For example, [22] compares the solutions for the cross section of a rivulet flowing down a plane obtained by solving the complete Navier-Stokes equation with the predictions of the lubrication approximation (see their Table I). For a contact angle of 30°, they find that the differences between the two approaches related with the shape of the free surface are of the order of few percent. Although the accuracy of lubrication approximation is not so good regarding the details of the velocity field, they find that these velocity differences cancel out when the total flux along the rivulet is computed. The issue of appropriateness of the use of lubrication approximation was also discussed earlier [23]. In that work it was shown that there are some differences in the free surface slope between lubrication theory and Stokes formulation, but only very close to the contact line.

Another concern regarding the use of lubrication approximation is that one typically (as we do here) approximates curvature of the free surface by h_{xx}, where x is in-plane coordinate. This issue was considered in [24], where it is shown that use of the complete nonlinear curvature yields only a few percent difference (see Fig.2b in [24]). There have been also some attempts [25, 26] to improve the typical lubrication approximation approach. These works show that including a correction factor to the flux term in the continuity equation extends the limits of its validity. Therefore, it may be appropriate to implement these improvements when precise quantitative results are desired. In the present problem, where we are mainly concerned with the basic mechanisms involved in the dewetting and breakup processes, we expect that standard lubrication approach is sufficient.

The van der Waals forces are included in the formulation of a lubrication model via disjoining pressure $\Pi(h)$ (see for instance [9]). The resulting equation for the fluid thickness, $h = h(x, y, t)$, is (see, e.g., [27, 15, 16])

$$3\mu\frac{\partial h}{\partial t} + \gamma\nabla\cdot\left(h^3\nabla\nabla^2 h\right) + \nabla\cdot\left[h^3\nabla\Pi(h)\right] - \rho g\nabla\cdot\left(h^3\nabla h\right) = 0, \tag{1}$$

where μ is the viscosity, ρ is the fluid density, γ is the surface tension, and g is the gravity. Here, the first term stands for viscous dissipation and the other three terms account for the driving forces, which are surface tension, van der Waals and gravity force, respectively. The disjoining pressure model that we use

$$\Pi(h) = \kappa f(h) = \kappa\left[\left(\frac{h_*}{h}\right)^n - \left(\frac{h_*}{h}\right)^m\right], \tag{2}$$

introduces κ (proportional to the Hamaker constant) and the exponents $n > m > 1$ (note that $f(h)$ is a dimensionless function). The first term represents liquid-solid repulsion, while the second term is attractive, leading to a stable film thickness $h = h_*$. Within this model, $\kappa = S/(Mh_*)$, where S is the spreading parameter, and $M = (n-m)/((m-1)(n-1))$ (see [9]). The spreading parameter can be related to the apparent contact angle θ via Laplace-Young condition $S = \gamma(1-\cos\theta)$.

Here, we take x-axis along the rivulet, and y-axis in the transverse direction. By defining the dimensionless variables $\tilde{h} = h/a$, $\tilde{x} = x/a$, $\tilde{y} = y/a$, $\tilde{t} = t/t_c$, with $t_c = 3\mu a/\gamma$, Eq. (1) becomes

$$\frac{\partial h}{\partial t} + \nabla\cdot\left(h^3\nabla\nabla^2 h\right) + K\nabla\cdot\left[h^3 f'\nabla h\right] - \nabla\cdot\left(h^3\nabla h\right) = 0, \tag{3}$$

where $f' = df/dh$ and we have omitted the 'hat' symbol for simplicity. We define $K = \kappa a/\gamma$, with $a = \sqrt{\gamma/\rho g}$ being the capillary length.

2.1. Steady state (base) solution

We first concentrate on the x-independent solution, $h(y,t)$, so that Eq. (3) reduces to

$$\frac{\partial h}{\partial t} + \frac{\partial}{\partial y}\left[h^3\left(\frac{\partial^3 h}{\partial y^3} + Kf'\frac{\partial h}{\partial y} - \frac{\partial h}{\partial y}\right)\right] = 0. \tag{4}$$

We consider now $\partial h/\partial t = 0$. After integrating twice the resulting equation and using the boundary conditions $h_0''' = h_0' = 0$ at $y = \pm\infty$, where the primes stand for y-derivatives, we obtain (see e.g. [9]):

$$h_0'' + Kf(h_0) - h_0 + p = 0, \tag{5}$$

where the constant $p > 0$ is the equilibrium pressure [28, 29] within the fluid. An analysis [28, 30, 9] of the solutions of Eq. (5) shows that there is a range of pressures $p_c < p < p^*$

for which there exist bounded-in-height solutions, where $h_{0,min} < h_0 < h_{0,max}$. Within that range, the value of p corresponds to different cross section areas,

$$A = 2\int_0^\infty (h_0(y) - h_{0,min})\, dy, \tag{6}$$

where [28, 9] $h_{0,min} \approx h_* + ph_*/K(n-m)$. Figure 2 shows relationship between p and the corresponding area, A. For the case considered here, with gravity effects included, p cannot be lower than a certain limit, p_c, and, consequently, the maximum drop thickness, $h_{0,max}$, is bounded from above.

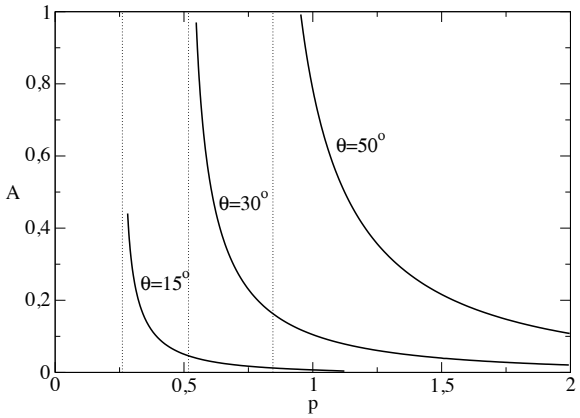

Figure 2. Relationship between pressure, p, in Eq. (5) and the corresponding area, A, of the rivulet cross section for three different contact angles, θ. Here, we use $n = 3$, $m = 2$ and $h_* = 10^{-2}$.

The solution of Eq. (5) is studied in detail in the Appendix B of [9]. The case with no van der Waals forces, i.e. $K = 0$, but supplemented with boundary condition $h = 0$ at the contact lines ($x = \pm w/2$, w being the width of the 1D drop) is also analyzed in that paper. Here, we use both solutions as possibilities to describe the cross section of the rivulets.

2.2. Perturbations and eigenvalue problem

In order to perform the linear stability analysis (LSA) of the transverse thickness profile, $h_0(y)$, with respect to longitudinal perturbations (x-direction), we write:

$$h(x, y, t) = h_0(y) + \epsilon g(y) \exp(\sigma t + ikx) \tag{7}$$

where ϵ is small number, $g(y)$ is the amplitude of the perturbation, $k = 2\pi/\lambda$ is the wave number, and λ is the wavelength.

By replacing Eq. (7) into Eq. (4), we obtain to $O(\epsilon)$ the eigenvalue problem:

$$\mathcal{L}g = -\sigma g$$

where $\mathcal{L}$ is the linear operator defined by:

$$\mathcal{L}g = c_4(y)g_{yyyy} + c_3(y)g_{yyy} + c_2(y)g_{yy} + c_1(y)g_y + c_0(y)g, \tag{8}$$

where the coefficients $c_i(y)$ $(i = 0, ..., 4)$ are defined by:

$$\begin{aligned} c_4(y) &= h_0^3, \\ c_3(y) &= 3h_0^2 h_0', \\ c_2(y) &= -\left(1 + 2k^2 - Kf'\right) h_0^3, \\ c_1(y) &= -h_0^2 \left[3(1 + k^2 - Kf') - 2h_0 K f''\right] h_0' \\ c_0(y) &= c_{0,2} h_0^2 + c_{0,3} h_0^3 + c_{0,4} h_0^4 \end{aligned} \tag{9}$$

and $c_{0,j}$ $(j = 2, 3, 4)$ are given by:

$$\begin{aligned} c_{0,2}(y) &= 3h_0'^2 K f'', \\ c_{0,3}(y) &= k^2\left(1 + k^2 - Kf'\right) - Kf''\left(p + Kf\right) + h_0'^2 K f'''' \\ c_{0,4}(y) &= Kf'' \end{aligned} \tag{10}$$

We use $n = 3$, $m = 2$, and $h_* = 0.01$. The considered contact angles range between $\theta = 30°$ and $\theta = 50°$.

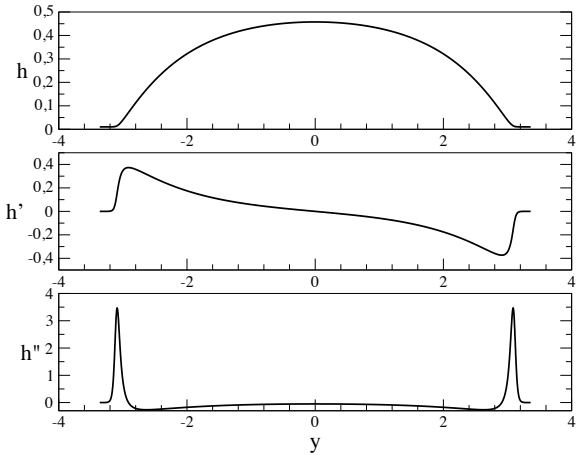

Figure 3. Profiles of (a) thickness, (b) slope and (c) curvature of a rivulet cross section for $A = 2$ and $\theta = 30°$.

Figure 3 shows the thickness, slope and curvature profiles for $A = 2$ and $\theta = 30°$. Figure 4 show the resulting dispersion relation curves. We see that the maximum growth rate as well as its corresponding wavenumber diminish as A is increased.

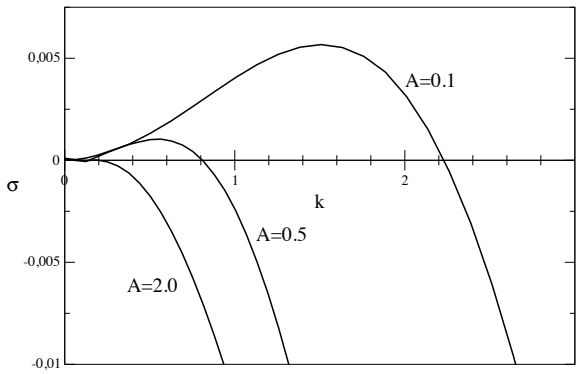

Figure 4. Dispersion relations for the three rivulet cross sections, A, using $\theta = 30°$.

3. 3D numerical simulations

In order to understand the nonlinear effects in the rivulet instability, we perform numerical simulations of the evolution of the rivulet governed by the full nonlinear Eq. (3). The calculations are carried out in a rectangular computational domain defined by $0 \leq x \leq X$ and $0 \leq y \leq Y$, which is divided into cells of size $\delta x \times \delta y$ (typically, we use $\delta_x = \delta_y = 0.04$). Equation (3) is discretized in space using a central finite difference scheme. Time discretization is performed using implicit Crank-Nicolson scheme. We note that all the results presented in this paper are fully converged, as verified by grid refinement; more details about numerical issues can be found in [31].

We choose a rivulet with pressure $p = 5$ and, due to the symmetry along the line $x = 0$, we simulate only half of the whole rivulet, i.e. $y > 0$. We take a numerical domain length, L, coincident with the wavelength of maximum growth, $\lambda_m = 1.087$ and impose no-flow (symmetry) conditions at the boundaries, which is equivalent to periodic boundary conditions for this infinite rivulet case. We perturb the free surface of the rivulet at $t = 0$ as prescribed by Eq. (7), and take $\epsilon = 10^{-3}$ and $g(y)$ as given by the corresponding (varicose) eigenfunction. Fig. 5 shows the time evolution of the free surface shape, where the breakup process is clearly observed at the middle of the domain.

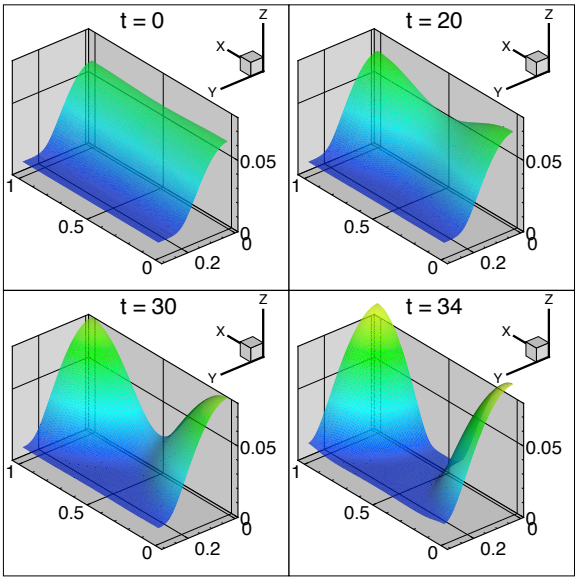

Figure 5. Evolution of a fluid rivulet of length $L = 1.087$ with $p = 5$. We employ a perturbation with wavelength $\lambda_m = 1.087$.

In Fig. 6 we show the amplitude of the perturbation in the middle of the rivulet, i.e., at $x = L/2$ and $y = 0$, measured as the difference between the maximum height of the rivulet and the fluid thickness at that point. For early times, the perturbation follows an exponential law, as expected for a linear regime. The good agreement between the exponent, β, that fits this behavior, and the eigenvalue σ corresponding to $\lambda_m = 1.087$ indicates that the eigenvalue problem describes correctly the early evolution of a given steady initial profile.

An interesting feature of this analysis is that a perturbation different from the corresponding eigenfunction, say by setting $g(y)$ in Eq. (7) equal to unity instead, yields a stable flow, i.e. the amplitude of the perturbation decreases and no rivulet breakup occurs.

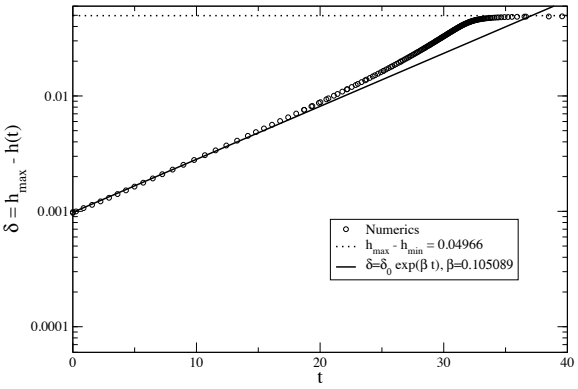

Figure 6. Evolution of the amplitude, δ, of the perturbation at $(x = L/2, y = 0)$ with $L = \lambda_m = 1.087$. Here, $\theta = 50°$ and $p = 5$.

Motivated by the comparison with experimental results in the following section, we here

analyze the evolution of finite length rivulets. Thus, we perform the numerical simulation for an initial condition obtained by modulating the steady solution of the rivulet as [9]:

$$h(x, y, 0) = h_0(y) \left[\arctan\left(q(x - x_1)\right) - \arctan\left(q(x - x_2)\right)\right]/\pi, \tag{11}$$

where x_1, x_2 are the coordinates of the end points of the rivulet, so that the fluid length is $\ell = x_2 - x_1$. The computational domain has an x-length $L = \ell/2 + 1$, i.e., half length of the rivulet plus a small space for the precursor film ahead of it. The value of q determines the width of the transition region between the unperturbed rivulet of height h_{apex} and the precursor film region. We use a relatively large q (typically, $q = 100$) to obtain an initial condition resembling a step function connecting $h_0(y)$ and h_* at the end points of the bulk.

The evolution of a finite length rivulet for $p = 5$ is shown in Fig. 7. This mechanism of rivulet breakup has previously been studied in connection with the one dimensional (1D) rupture of flat thin films [9, 32]. In those cases, there exist instabilities of two different kinds: spinodal or nucleation instability. These regimes depend on the value of the thickness of the film, with nucleation being relevant for thinner films. The main difference between the final patterns formed by these two mechanisms is the distance, D, between consecutive 1D-drops. In the spinodal regime, D is given by the wavelength, λ_m, of maximum growth rate of the corresponding LSA, while in the nucleation regime D is not correlated with λ_m, but it is determined by the nonlinear evolution of the flow.

In the 3D-rivulet case, its thickness $h_{apex} = h_0(0)$ depends on the value of the pressure, p, inside the rivulet. In particular, for $p = 5$, we find that $D \approx 1.09$, which is very close to λ_m. We find basically the same result for other values of p, so that we conclude:

$$D \approx \lambda_m \tag{12}$$

for different rivulet thicknesses h_{apex}. This indicates that no nucleation regime exists in the rivulet problem and, therefore, the distance between droplets is close to the wavelength of the maximum growth resulting from LSA, λ_m.

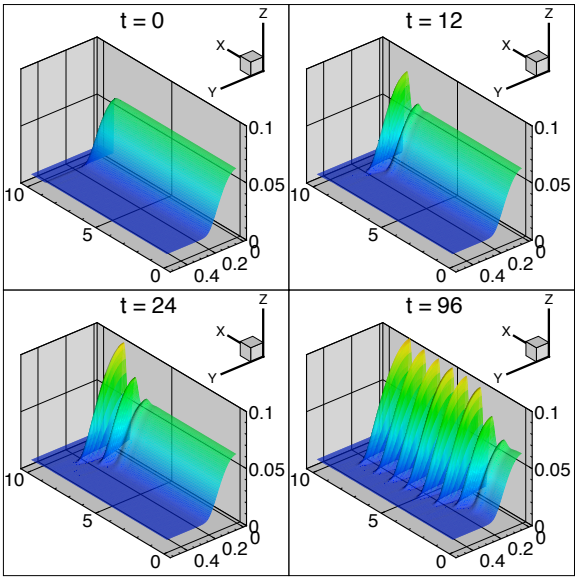

Figure 7. Evolution of a finite rivulet of length $L = 18$ with $p = 5$. The final pattern is formed by droplets separated an average distance $D = 1.03$.

The time needed for surface perturbations, like that used in LSA, Eq. (7), to break up the rivulet is given by $t_s = -\ln \epsilon/\sigma_m$. In this case, we have $\sigma_m = 0.114$, so that surface perturbations of amplitude $\epsilon = 10^{-3}$ lead to breakup only for $t_s = 60$. Thus, for the considered rivulet length, breakup due to dewetting from the rivulet ends proceeds faster than surface perturbations have time to grow.

4. Comparison with experimental results

In this section we aim to compare the LSA results, as well as from 3D-numerical simulations, for the evolution of the rivulet instability with the experiments reported by González et al. [33]. In that work, the rivulet is formed by capturing a thin jet of silicon oil (polydimethysiloxane, PDMS) on a coated glass slide, which is a partially wetting surface for the oil. The evolution of this rivulet shows a repetitive process of length contraction and breakup into droplets (see Fig. 8). Each experiment is characterized by a contact angle, θ, and the cross sectional area of the rivulet, A. When the fluid is placed on the substrate, the initial width, w, of the rivulet is also measured and reported in that work. Thus, the theoretical model used to describe this initial configuration must be able to yield w for given θ and A. Since here we use the capillary length a ($= 0.145\ cm$ for PDMS), as a characteristic length scale, we write the main experimental results reported in González et al. [33] in units of a (see Table 1). The last column in Table 1 corresponds to the predictions given in [13]. We observe large difference between the experiment and that theoretical result.

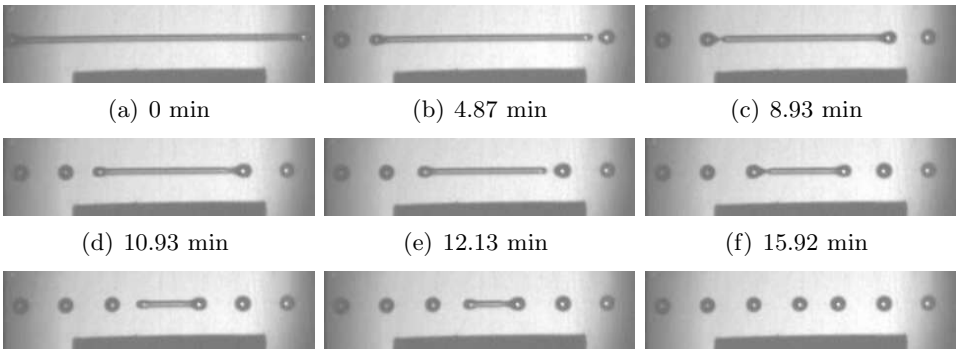

(a) 0 min (b) 4.87 min (c) 8.93 min

(d) 10.93 min (e) 12.13 min (f) 15.92 min

(g) 17.83 min (h) 19.33 min (i) 22.95 min

Figure 8. Evolution of a silicon oil rivulet of length 7 cm on a substrate covered with EGC–1700 ($\theta_e = 57°$) as reported by González et al. [33] and formation of primary drops. The black segment corresponds to 4.2 cm.

Table 1. The first six columns correspond to the experimental data reported in Table I of González et al. [33], where w is the rivulet width and n is the number of drops in the rivulet of length $L = 50$ (in units of a). The last column shows λ_m predicted by the results in [13].

Exp.	θ	A	w	n	D_{exp}	λ_m [13]
1	57°	0.069	0.517	12	3.501	1.015
2	57°	0.296	1.076	4	12.84	2.113
3	57°	0.316	1.110	3	19.53	2.213
4	63°	0.041	0.352	16	2.802	0.701
5	63°	0.296	0.993	7	6.117	1.980

Next, we compare the values of λ_m given by LSA presented here, with the experimental distance between drops, D_{exp}. To do so, we obtain the base thickness profile by using the solution of Eq. (5) with van der Waals and gravity forces. Since this solution is determined by a fixed value of the pressure, p, inside the drop, we find the corresponding p by relating it with the experimental drop area, A, which is defined as the area for $h > h_*$ in the theoretical profile.

The values of λ_m reported in Table 2 are obtained for these values of p and for θ as given by the experimental data for few different values of the exponents (n, m). These results are closer to the experimental data than the results from [13], but there is still only qualitative agreement. It should be noted that the discrepancy is particularly large in the cases when only few drops are seen, and the statistical fluctuations of the experimental results may be large. We also note that the influence of the exponents (n, m) in van der Waals model is relatively weak.

Table 2. Comparison of D_{exp} with λ_m as obtained from LSA for a cross section with van der Waals and gravity forces by using few different pairs of (n, m).

D_{exp}	$\lambda_m^{(3,2)}$	$\lambda_m^{(4,3)}$
3.501	2.424	2.356
12.84	5.427	4.885
19.53	5.694	5.136
2.802	1.743	1.742
6.117	5.178	4.700

We believe that one reason for the relatively larger discrepancy between the values of D_{exp} and λ_m is the differences between the rivulet widths, w, of the base solution profile used in LSA, and the corresponding measured values reported in Table 1 (see Fig. 9a). These departures come from the inability of this base profile to yield large values of contact angles at the inflection points, as explained in Appendix A. In fact, the experimental values of the contact angle refer to the slope at these points, since they are measured by the maximum deviation of a light beam perpendicular to the substrate. Consequently, when we set θ equal to the values reported in [33], the profiles with van der Waals forces (as those used in LSA for Table 2) exhibit apparent contact angles different to those experimentally measured.

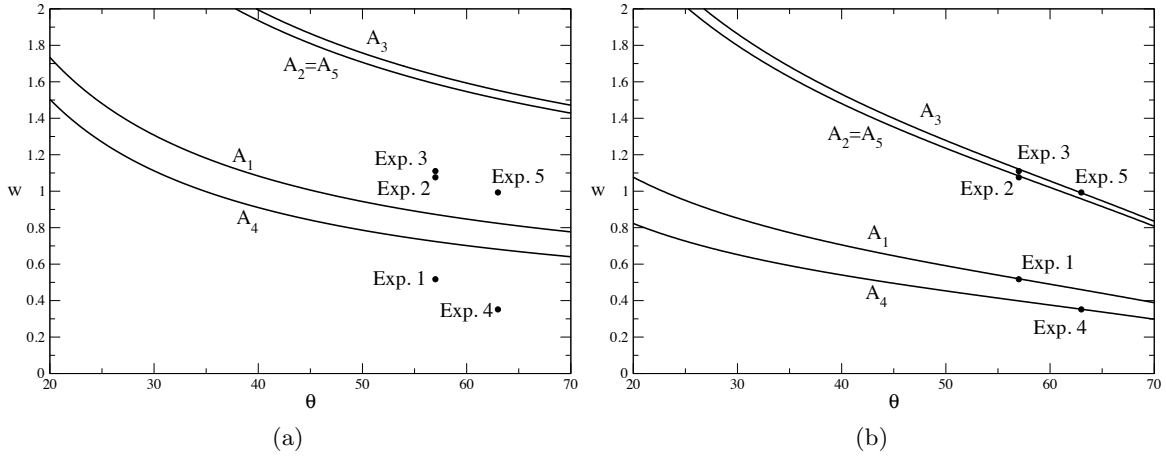

Figure 9. Width of the rivulet, w, as a function of contact angle, θ, as given by the solution: (a) with and (b) without van der Waals forces. The symbols correspond to five experimental cases reported in [33].

On the other hand, we find that the steady solution of a drop *without* considering van der Waals forces (see e.g. Appendix B in [9]) yields very accurate values of w when compared with experiments (Fig. 9b). It is worth noting that the LSA performed by using the base solution

without van der Waals forces yields stability for zigzag modes and only marginal instability ($\sigma = 0$) for varicose modes for all $k > 0$.

Thus, we perform three dimensional (3D) numerical simulations with an initial condition as given by the solution *without* van der Waals forces. We start the evolution with the same area, contact angle and width as in the experiments, which assures an initial condition close to the experimental one. The evolution must be performed with the inclusion of van der Waals forces, since they are necessary to account for the partial wetting condition. An example of this evolution is shown in Fig. 10 for experiment 2.

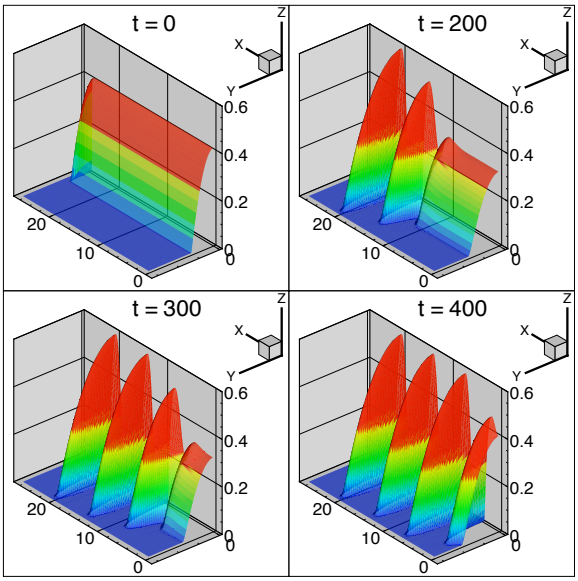

Figure 10. Evolution of experiment 2 of Table 2 with initial condition *without* van der Waals forces, so that A, θ and w are given by the values in second line of Table 2. The final pattern is formed by droplets separated an average distance $D_{num} = 6.6$.

The average distance between drops obtained for all experimental cases reported in [33] are shown as D_{num} in Table 3. Clearly, regardless of the choice of exponents, the large differences with the experimental data where only small number of drops is present, similarly to the results shown in Table 2. It should be also noted that both λ_m and D_{num} are calculated using relatively thick precursor film ($h_* = 0.01$. This large value, required due to significant computational cost involved if thinner precursor were used, may also contribute to inaccuracy of the results.

Table 3. Distance between drops, D_{num}, from numerical simulations for (n, m) equal to $(3, 2)$ and $(4, 3)$ compared with the experimental values from Table 1.

D_{exp}	$D_{num}^{(3,2)}$	$D_{num}^{(4,3)}$
3.501	2.745	3.936
12.84	6.600	9.600
19.53	7.000	7.080
2.802	1.754	2.730
6.117	7.200	7.080

5. Conclusions

The linear stability analysis (LSA) of partially wetting fluid rivulets has proved to be very useful for a deeper understanding of the breakup process. On one hand, it allows to consider

simultaneously the effects of wettability and gravity. Therefore, it constitutes an advantage with respect to previous approaches, which are limited to a circular cross section and sharp contact lines with imposed contact angles. A more detailed comparison of our LSA results with those theories is out of the scope of this work and will be presented elsewhere. On the other hand, we have shown that the results of LSA apply also to large perturbations - therefore, the wavelength of maximum growth rate determines the distance between drops after breakup.

The comparison of the predictions obtained from both LSA and 3D numerical simulations has opened some challenging issues. The fact that: (a) for given area and contact angle the width of the rivulet given by the profile with van der Waals forces does not agree with experimental measurements (cf. Fig. 9a), and (b) that relatively large contact angles cannot be reached by the cross section profile with intermolecular forces considered here (see Appendix A), indicate intrinsic limitations of this lubrication approach. Future work is required to fully understand the breakup of a partially wetting rivulet on horizontal substrate.

Appendix A. Rivulet width and apparent contact angle

In this Appendix we show a peculiar feature of the steady state solution for the cross section of the rivulet. The value of the contact angle, θ, that characterizes the wettability of the substrate is introduced in the theory by means of the prefactor K in the van der Waals potential. Let us recall [27, 9] that the dependence of K on θ is obtained by performing a local analysis in the contact line region (which matches onto the precursor film of thickness h_*) and assuming that far away from that location the thickness profile asymptotes to a linear behavior with slope θ. However, the calculation of a profile that includes a maximum thickness at a finite distance from that region does not completely satisfies this assumption. This case unavoidably has an inflection point that connects the region near the precursor with that in the neighborhood of the apex (bulk). Thus, the actual contact angle is basically given by the slope at the inflection point, θ_i.

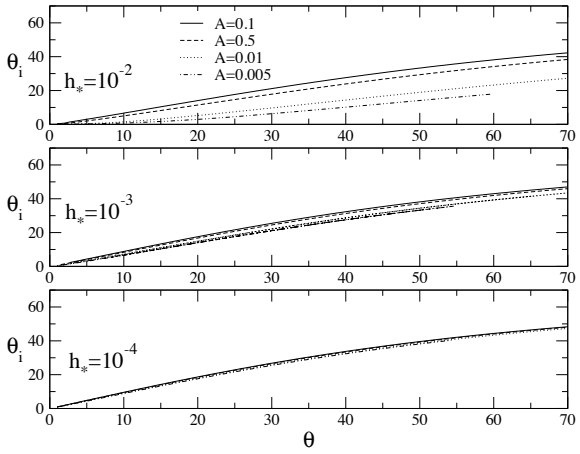

Figure A1. Slope at the inflection point (apparent contact angle) as a function of the contact angle used to determine prefactor K in van der Waals term, for typical areas A's. No gravity effects are considered here.

The analysis of the solutions of Eq. (5) allows to obtain the relationship between θ_i and θ for given area, A (or equivalently, given pressure p) as shown in Fig. A1. We see that, even for very large θ, θ_i cannot reach this high value, but it saturates around 50° (these θ_i's are calculated without including gravitational effects, but these are not of relevance to the present discussion). All the curves collapse into a single one as $h_* \to 0$, thus showing that the difference between θ_i and θ is only due to the fact that the drop width is finite. This result is an important drawback since these large apparent contact angles cannot actually be reached by the theory with the commonly used van der Waals model.

Acknowledgements. J.A.D. and A.G.G. thank support from Consejo Nacional de Investigaciones Científicas y Técnicas de la República Argentina (CONICET) and from Agencia Nacional de Promoción Científica y Tecnológica (ANPCyT) through grant PICTR 0094/02.

References

[1] Stone H, Stroock A and Ajdari A 2004 *Ann. Rev. Fluid Mech.* **36** 381
[2] Stone H A and Kim S 2001 *AIChE J.* **47** 1250
[3] Ruschak K 1999 *Ann. Rev. Fluid Mech.* **17** 65
[4] Kheshgi H S 1997 *Liquid Film Coating* ed Kistler S F and Scheizer P M (London: Chapman and Hall) p 183
[5] Larson R G and Regh T J 1997 *Liquid Film Coating* ed Kistler S F and Scheizer P M (London: Chapman and Hall) p 709
[6] Becker J, Grün G, Seemann R, Mantz H, Jacobs K, Mecke K R and Blossey R 2003 *Nature Mat.* **2** 59
[7] Brochard-Wyart F and Redon C 1992 *Langmuir* **8** 2324
[8] Herminghaus S, Jacobs K, Mecke K, Bischof J, Fery A, Ibn-Elhaj M and Schlagowski S 1998 *Science* **282** 916
[9] Diez J A and Kondic L 2007 *Phys. Fluids* **19** 072107
[10] Favazza C, Kalyanaraman R and Sureshkumar R *Nanotechnology* **17** 4229
[11] Davis S H 1980 *J. Fluid. Mech.* **98** 225
[12] Langbein D 1990 *J. Fluid. Mech.* **213** 251
[13] Roy R V and Schwartz L W 1999 *J. Fluid. Mech.* **391** 293
[14] Sekimoto K, Oguma R and Kawasaki K 1987 *Annals of Physics* **176** 359
[15] Schwartz L W and Eley R R 1998 *J. Colloid Interface Sci.* **202** 173
[16] Schwartz L, Roy R, Eley R and Petrash S 2001 *J. Colloid Interface Sci.* **234** 363
[17] Glasner K B 2003 *Phys. Fluids* **15** 1837
[18] Pismen L M and Rubinstein B Y 2000 *Phys. Fluids* **12** 480
[19] Pismen L M and Pomeau Y 2000 *Phys. Rev. E* **62** 2480
[20] Davis J M and Troian S M 2003 *Phys. Rev. E* **67** 016308
[21] Pismen L M and Thiele U 2006 *Phys. Fluids* **18** 042104
[22] Perazzo C A and Gratton J 2004 *J. Fluid Mech.* **507** 367
[23] Goodwin R and Homsy G M 1991 *Phys. Fluids A.* **3** 515
[24] Münch A and Wagner B 2005 *Physica D* **209** 178
[25] Snoeijer J H 2006 *Physics Fluids* **18** 021701
[26] Hirasaki G J and Yang S Y 2002 *Contact Angle, Wettability and Adhesion* **2** 1–30
[27] Oron A, Davis S H and Bankoff S G 1997 *Rev. Mod. Phys.* **69** 931
[28] Glasner K B and Witelski T P 2003 *Phys. Rev. E* **67** 016302
[29] Bertozzi A L, Grün G and Witelski T P 2001 *Nonlinearity* **14** 1569
[30] Glasner K B and Witelski T P 2005 *Physica D* **209** 80
[31] Diez J and Kondic L 2002 *J. Comp. Phys.* **183** 274
[32] Thiele U, Velarde M G, Neuffer K and Pomeau Y 2001 *Phys. Rev. E* **64** 031602
[33] González A G, Diez J, Gratton R and Gomba J 2007 *Europhysics Letters* **77** 44001